

Crosswell tomographic estimation of elastic constants in heterogeneous transversely isotropic media

Reinaldo J. Michelena*, Jerry M. Harris‡, and Francis Muir‡

ABSTRACT

The procedure to estimate elastic constants of a transversely isotropic medium from limited-aperture traveltimes has two steps. First, P - and SV -wave traveltimes are fitted with elliptical velocity functions around one of the axes of symmetry. Second, the parameters that describe the elliptical velocity functions are transformed analytically into elastic constants. When the medium is heterogeneous, the process of fitting the traveltimes with elliptical velocity functions is performed tomographically, and the transformation to elastic constants is performed locally at each position in space. Crosswell synthetic and field data examples show that the procedure is accurate as long as the data aperture is constrained as follows: it should not be too large otherwise the elliptical approximation may not be adequate, and it should not be too small because the tomographic estimation of elliptical velocities fails, even if the medium is actually isotropic.

INTRODUCTION

Recent papers have addressed the problem of estimating velocity anisotropy from crosswell measurements using ray theoretic traveltime tomography. These papers have focused on the problem of eliminating the artifacts obtained when isotropic tomography is used to invert data recorded in anisotropic environments (Carrion et al., 1992). McCann et al. (1989) show how an isotropic inversion improved after assuming a fixed amount of anisotropy. Stewart (1988) and Williamson et al. (1993) describe heterogeneities with nonoverlapping square cells and the velocity anisotropy using Thomsen's (1986) expression for P -wave phase velocity in weakly anisotropic media. Saito (1991) and Lines

(1992) propose to separate the effects of anisotropy and heterogeneity by first "removing" the anisotropy effects from the data so that conventional isotropic tomography in heterogeneous media can later be applied. The elimination of the anisotropy effect is partial and depends on the model of heterogeneities that is assumed. Qin et al. (1992) describe the model as a superposition of two parts, one isotropic and the other anisotropic. The heterogeneities in the isotropic part are described by small, square cells, and the heterogeneities in the anisotropic part are described by large cells. By using raypaths computed in isotropic models for the anisotropic inversion, Qin et al. (1992) implicitly also assume that the medium is weakly anisotropic. Chapman and Pratt (1992) and Pratt and Chapman (1992) also assume weak anisotropy but make no assumption about the type of anisotropy or heterogeneity. Pratt and Chapman's procedure is more complex for shear waves than for compressional waves, and it requires, as do all the previous methods, wide-aperture data.

The preceding papers (except Saito's) assume weakly anisotropic media to justify ray tracing in isotropic models. The assumption of weak anisotropy also justifies the use of Thomsen's equation for P -wave phase velocity to approximate the corresponding group velocity [in the papers by Stewart (1988), Lines (1992), and Williamson et al. (1993)]. No assumptions are made about the heterogeneities [except in Saito's (1991) paper], which makes an accurate estimation of spatial variations in velocity anisotropy more difficult. Although all these papers show how to alleviate artifacts in the tomograms by estimating parameters that describe variations of velocity with direction, none of them show how to transform those parameters into the five elastic constants that describe a general transversely isotropic (TI) medium.

This paper focuses on the estimation of the elastic constants that describe heterogeneous TI media when the measurements, direct-arrival traveltimes, have a narrow aperture around one axis of symmetry. We start by reviewing the solution to the problem for homogeneous media given by Michelena (1994). Then we show that the generalization to

Manuscript received by the Editor June 1, 1993; revised manuscript received May 6, 1994.

*Formerly Dept. of Geophysics, Stanford University, Stanford, CA 94305; presently INTEVEP, S.A., P.O. Box 76343, Caracas 1070A, Venezuela.

‡Department of Geophysics, Stanford University, Stanford, CA 94305.

© 1995 Society of Exploration Geophysicists. All rights reserved.

heterogeneous media consists of fitting the data with heterogeneous elliptically anisotropic models that can be transformed into models for elastic constants. No assumptions are made about the weakness of the anisotropy, or the heterogeneity, and rays are traced in heterogeneous anisotropic models. Synthetic and field data examples show that the technique works well for simple structures with small dips, but since only limited-aperture data are used, we expect the technique to produce less accurate results when the medium contains arbitrary 2-D structures.

The data aperture is constrained in two different ways. First, it should not be too small to ensure that there is enough curvature to estimate the normal moveout velocities. Second, it should not be too wide to ensure that the elliptical fit remains accurate for the given wave type. We show the application of the technique using synthetic *P*- and *SV*-wave traveltimes generated through a heterogeneous TI model under the proper constraints. In this example, since no *SH*-waves are used, only four elastic constants can be estimated. Finally, we present a field data example from a west Texas oil field. This final example shows how the estimation of the elastic constants can add useful information when we study the properties of reservoir and nonreservoir rocks.

FROM TRAVELTIMES TO ELASTIC CONSTANTS: REVIEW

As shown in Michelena (1994), obtaining the elastic constants of a homogeneous TI medium from *P*-, *SV*-, and *SH*-wave traveltimes around the horizontal axis (assuming vertical axis of symmetry) is a two-step procedure. The first step is to obtain direct and normal moveout (NMO) velocities by separately fitting traveltimes from each wave type with ray velocity functions of the form

$$t^2 = \Delta x^2 S_x^2 + \Delta z^2 S_{z,NMO}^2, \tag{1}$$

where *t* is the traveltime, and *S_x* and *S_{z,NMO}* are the horizontal and vertical NMO slownesses of the best fitting ellipse around the horizontal axis. The parameters Δx and Δz determine the distance ($d = \sqrt{\Delta x^2 + \Delta z^2}$) between two points for a ray that travels in the homogeneous medium.

The second step is to map these elliptical velocities into elastic constants (in units of velocity squared) by using the following relations:

$$W_{11} = W_{P,x}, \tag{2}$$

$$W_{44} = W_{SV,x} \tag{3}$$

$$W_{13} = \sqrt{(W_{P,zNMO} - W_{SV,x})(W_{P,x} - W_{SV,x})} - W_{SV,x}, \tag{4}$$

$$W_{33} = W_{SV,zNMO} + W_{P,zNMO} - W_{SV,x}, \tag{5}$$

$$W_{66} = W_{SH,x}, \tag{6}$$

where $W_{ij} = c_{ij}/\rho$, the elastic moduli divided by density. $W_{P,x}$, $W_{P,zNMO}$, $W_{SV,x}$, $W_{SV,zNMO}$, $W_{SH,x}$, and $W_{SH,zNMO}$ are the direct or NMO-phase velocity squared for *P*-, *SV*-, and *SH*-waves. In the rest of the paper, we refer to these velocities as W_* , which are estimated from the relation

$$W_* = \frac{1}{S_*^2}. \tag{7}$$

The corresponding equations for near vertical propagation (VSP) can be obtained by interchanging *x* and *z*, and W_{11} and W_{33} in equations (2) to (5).

When the medium is heterogeneous, the elastic constants can be estimated by applying the procedure for homogeneous media many times to a heterogeneous model described as a superposition of homogeneous blocks. These blocks should incorporate our previous knowledge about the structure. The direct and NMO velocities needed at each block are estimated tomographically, as explained in the following section.

Tomographic estimation of elliptical velocities

Figure 1 shows the type of model we will consider in this paper to do the tomography step necessary in the estimation of the elastic constants. The model consists of homogeneous elliptically anisotropic blocks with an axis of symmetry forming an angle γ_j with the vertical. The blocks are separated by straight interfaces of variable dip (*a_j*) and intercept (*b_j*). The expression for the traveltime *t_{i,j}* of the *i*th ray in the *j*th cell is a simple generalization of equation (1) (Michelena, 1993)

$$t_{i,j} = \sqrt{\Delta X_{i,j}^2 S_{\perp j}^2 + \Delta Z_{i,j}^2 S_{\parallel j}^2}, \tag{8}$$

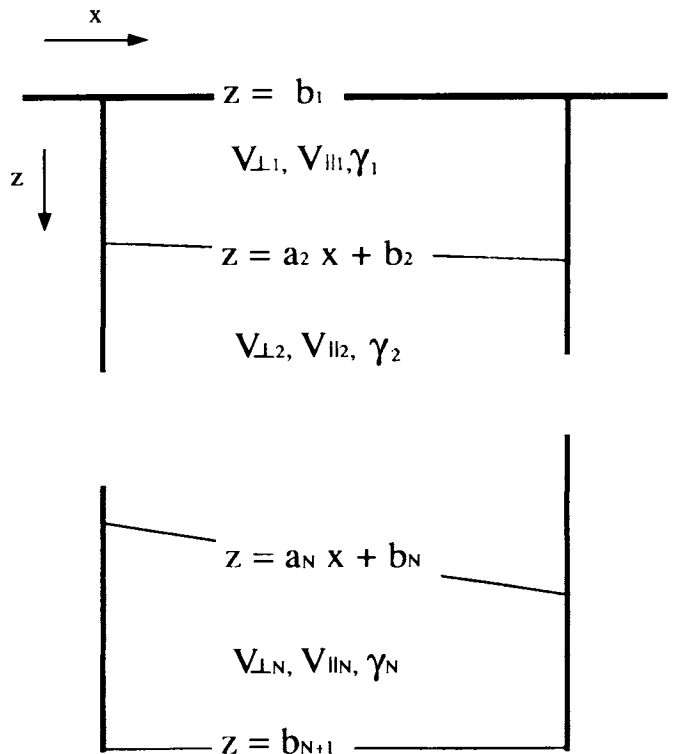


FIG. 1. Model of velocities and heterogeneities. The top and bottom interfaces are horizontal ($a_1 = a_{N+1} = 0$) and located at known depths.

where $S_{\perp j} = 1/V_{\perp j}$ and $S_{\parallel j} = 1/V_{\parallel j}$ are the slownesses in the directions perpendicular and parallel, respectively, to the axis of symmetry, and $\Delta X_{i,j}$ and $\Delta Z_{i,j}$ are

$$\begin{aligned}\Delta X_{i,j} &= \Delta x_{i,j} \cos \gamma_j \\ &\quad + (a_{j+1}x_{i,j+1} + b_{j+1} - a_j x_{i,j} - b_j) \sin \gamma_j, \\ \Delta Z_{i,j} &= -(a_{j+1}x_{i,j+1} + b_{j+1} - a_j x_{i,j} - b_j) \\ &\quad \times \cos \gamma_j + \Delta x_{i,j} \sin \gamma_j.\end{aligned}$$

In the previous expressions, $(x_{i,j}, z_{i,j})$ is the point of intersection between the i th ray and the j th interface. The quantity $\Delta x_{i,j}$ is defined as $\Delta x_{i,j} = x_{i,j+1} - x_{i,j}$.

The total traveltime for a ray that travels from source to receiver is

$$t_i(\mathbf{m}) = \sum_{j=1}^N t_{i,j}(\mathbf{m}) \quad i = 1, \dots, M, \quad (9)$$

where \mathbf{m} is the vector of model parameters of $5N$ elements:

$$\begin{aligned}\mathbf{m} &= (m_1, \dots, m_N, m_{N+1}, \dots, m_{2N}, m_{2N+1}, \dots, m_{3N}, \\ &\quad m_{3N+1}, \dots, m_{4N}, m_{4N+1}, \dots, m_{5N}) \\ &= (S_{\perp 1}, \dots, S_{\perp N}, S_{\parallel 1}, \dots, S_{\parallel N}, \\ &\quad \gamma_1, \dots, \gamma_N, b_1, \dots, b_N, a_1, \dots, a_N),\end{aligned}$$

and M is the total number of traveltimes.

Equation (9) is the system of nonlinear equations that relates the model parameters to the measured traveltimes. A linearized version of these equations is used to solve the inverse problem.

APERTURE CONSTRAINTS: CONSEQUENCES

As explained in the previous review section, the procedure for estimating elastic constants from P -, SV -, and SH -wave traveltimes can be summarized as tomographic estimation of elliptical velocities and transformation of the elliptical velocities into elastic constants. These two steps have opposite requirements in terms of data aperture. On the one hand, the mapping from elliptical velocities to elastic constants requires velocities estimated from rays that travel as closely as possible to one axis of symmetry (Michelena, 1994). On the other hand, the tomographic estimation of elliptical velocities requires wide ray angles to improve the conditioning of the problem, the accuracy of the NMO velocities, and the spatial resolution of the result. Therefore, the aperture of the traveltimes used for the inversion should satisfy the following two conditions simultaneously: it should not be too large otherwise the elliptical approximation may not be adequate, and it should not be too small because the tomographic estimation of elliptical velocities fails, even if the medium is actually isotropic. These two constraints are analogous to the constraints applied in surface geometries to the offsets of the reflection events used to estimate root-mean-square (rms) velocities from stacking velocities (Al-Chalabi, 1973; Yilmaz, 1987).

Large ray angles are important for the estimation of moderate and large dips in the medium. Since the procedure

does not allow the use of large ray angles in the inversion of P - and SV -wave traveltimes, we assume that the dips in the medium are small. If the dips are not small, they can be estimated first from SH -wave, wide-aperture traveltimes (that are truly elliptical), and the result can be used to constrain the boundaries in the inversion of P - and SV -wave data.

The axes of symmetry of the different homogeneous blocks that describe the model are assumed to be vertical or near vertical. [They can also be horizontal or near horizontal. The algorithm works equally well in either case because the axes of symmetry of the ellipses are not constrained to be either the major or the minor axis, as explained in Michelena (1993).] Therefore, when starting the iterations in the anisotropic traveltime tomography by assuming vertical axes of symmetry, it is possible to accurately estimate both the real inclinations of the axes of symmetry of the medium, and the elliptical velocities, regardless of the wave type. If the axes of symmetry are neither vertical nor close to vertical, we need to find their inclination first by fitting SH -wave traveltimes with heterogeneous elliptically anisotropic models, as explained in Michelena (1993). Once the inclination of the axes of symmetry of the different blocks is known, the elliptical group velocities of P - and SV -waves at each block are estimated using only rays that travel near the axes of symmetry. This process assumes also that the axes of symmetry of the different blocks are in the same plane of the survey.

In summary, in the absence of SH -wave traveltimes, the medium is assumed to have only small dips with axes of symmetry nearly vertical (or nearly horizontal). (The algorithm works equally well in both cases.) Large variations from this initial guess require elliptical SH -wave traveltimes that allow the use of larger data apertures. Hence the importance of recording three-component data sets.

When the inclination of the axes of symmetry varies across the medium, the estimated elastic constants are referred to different coordinate frames, one for each different axis of symmetry. For purposes of interpretation, having the elastic constants referred to different frames is not a problem as long as we also use the inclination of the axes of symmetry. However, for further computations (finite-difference modeling, for example) it might be necessary to transform the elastic constants to a common frame. This transformation can be done by using Bond's matrices (Auld, 1990).

SYNTHETIC EXAMPLE

P - and SV -wave synthetic traveltimes were generated using the anisotropic ray-tracing algorithm described in Michelena (1993). Figure 2 shows the heterogeneous TI model where the rays were traced. This model shows the variation in depth of $V_{ij} = \sqrt{W_{ij}}$. The crosswell geometry used to compute the traveltimes consists of 92 sources and 92 receivers at each well. The distance between wells is 390 ft (119 m), and the separations between consecutive sources or receivers is 23 ft (7 m).

Since the elastic constants of the medium are known, the corresponding elliptical velocities ($V_{P,x}$, $V_{P,z\text{NMO}}$, $V_{SV,x}$, and $V_{SV,z\text{NMO}}$) can be calculated by using the relations (2) to (5). Figure 3 shows the result. These velocities can be used to check how the algorithm performs in the first step toward

the estimation of the elastic constants, that is, the tomographic estimation of the elliptical velocities.

The paraxial elliptical approximation around the horizontal axis (assuming vertical axis of symmetry) is accurate for angles of less than $\approx 30^\circ$ (Michelena, 1994). For this reason, the inversion uses only rays whose angle measured from the horizontal satisfies this condition. However, no approximation is made in the computation of the synthetic traveltimes through the model of Figure 2. The paraxial approximation is made only during the inversion procedure in which the rays are traced in elliptically anisotropic instead of transversely isotropic models.

The fact that the straight line that connects a source-receiver pair forms a small angle with respect to the horizontal does not necessarily mean that the angle of the corresponding raypath is also small. The angle of the raypath increases in low-velocity layers and decreases in high-velocity layers. However, if the velocity contrasts are not too strong, it should be enough to look at the straight line that connects source and receiver to select the rays that satisfy the proper constraints.

Figure 4 shows the result of inverting the P -wave traveltimes. This figure also shows the theoretical elliptical velocities calculated from the elastic constants. The estimation of the horizontal P -wave velocity is, as expected, almost perfect, whereas the vertical NMO velocity is slightly overestimated ($\approx 3\%$) in all layers. As Figure 5 shows, the estimation of the

vertical NMO velocity is more accurate when inverting SV -wave traveltimes than when inverting P -wave traveltimes, which means that, for the range of ray angles used, the elliptical approximation works better for SV -waves than for P -waves. The error in $V_{SV,zNMO}$ is less than one percent.

When the medium is truly elliptical, the estimation of the NMO velocities is accurate as shown by Michelena et al. (1993). However, when fitting elliptical models to a more general TI medium, we see errors in the NMO velocities $V_{P,zNMO}$ and $V_{SV,zNMO}$ because the ray angles used are not sufficiently small.

The variation with depth in the theoretical P - and SV -wave elliptical velocities has been estimated accurately. Therefore, by using these two models of elliptical velocities and relations (2) to (5) at every depth, we can also expect an accurate estimation of the elastic constants as Figure 6 shows.

Since P - and SV -wave traveltimes are inverted separately and the interfaces are not constrained to move consistently with both data sets, the models obtained for P - and SV -wave elliptical velocities may not have all the interfaces at exactly the same depths. As a consequence, artificial thin layers (spikes) may appear when we estimate the elastic constants because there may be slight relative mispositions of the same boundaries in the two models. In Figure 6 these spikes are removed by applying a median filter to the elastic constants after the mapping from elliptical velocities. Another way to solve this problem is by describing the interfaces with the

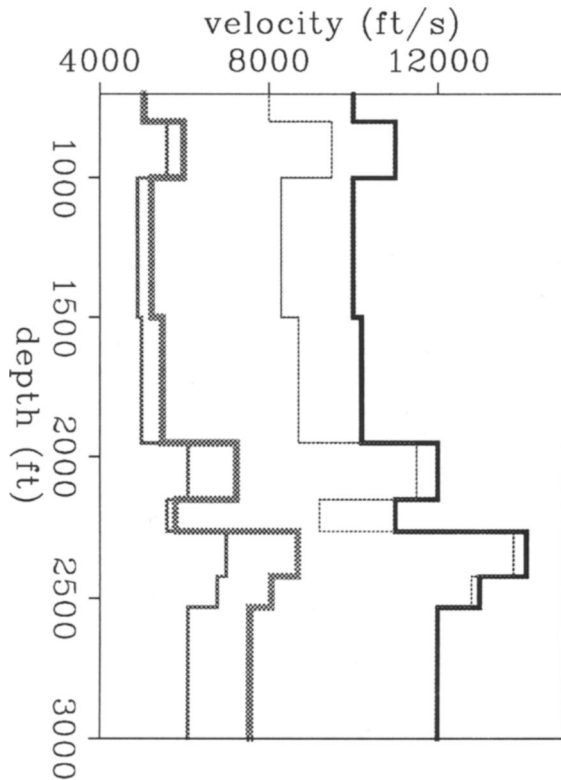


FIG. 2. Layered TI synthetic model. From left to right the four curves represent the elastic constants in units of velocity V_{44} , V_{13} , V_{33} , and V_{11} , respectively. The density is assumed to be unity.

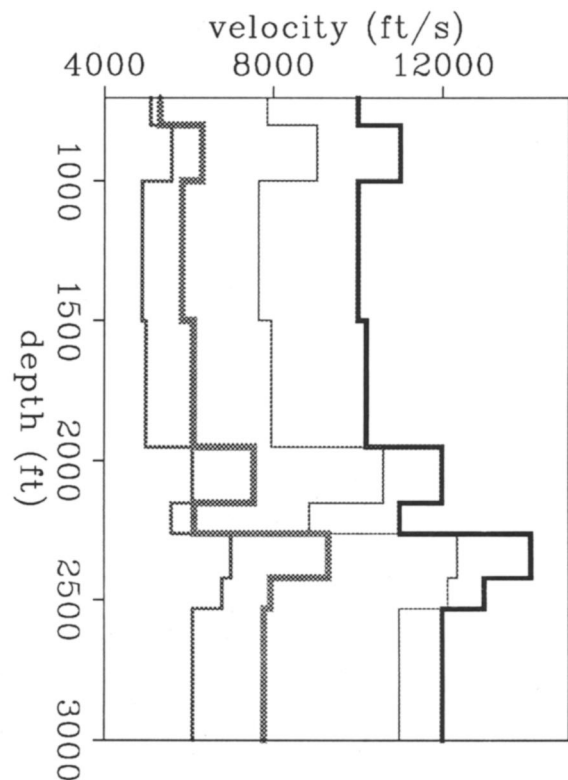


FIG. 3. Theoretical elliptical velocities around the horizontal axis calculated from the elastic constants shown in Figure 2. From left to right the four curves represent $V_{SV,x}$, $V_{SV,zNMO}$, $V_{P,zNMO}$, and $V_{P,x}$, respectively.

same parameters for both P - and SV -wave velocity models and inverting the two sets of traveltimes simultaneously.

Depending on the radiation pattern of the source, traveltimes that correspond to nearly horizontal rays may not always be available for either P - or SV -waves. When this happens, it may be necessary to use ray angles that are far from the horizontal because nothing else is available. Figure 7 shows an example where SV -wave elliptical velocities have been estimated by using ray angles between 28 and 36°. The estimated horizontal component of the velocity is as accurate as in Figure 5 even though this component is not well sampled by the raypaths used. The error in $V_{SV,zNMO}$ increases when using larger ray angles. However, as Figure 8 indicates, the error in the estimation of the elastic constants is still small because the P -wave elliptical velocities were estimated using small ray angles.

In the field data example that follows, SV -wave traveltimes are not available for small vertical offsets.

FIELD DATA EXAMPLE

Crosswell data were recorded at the McElroy Field, a carbonate reservoir of the Permian Basin in west Texas. This field has large oil reserves, it was discovered in 1926, and has been under continuous water-flooding since the early 1960s. McElroy Field produces mainly from intertidal and shallow-shelf dolostones and siltstones of the Grayburg Formation, which is a stratigraphic/structural trap. Hydraulic fracturing

has stimulated reservoir performance. Porosity and permeability data from cores show that the Grayburg Formation is very heterogeneous, with significant changes over short distances. One reason for the heterogeneity is that anhydrite and gypsum have plugged the pores (Avasthi et al., 1991). Structurally, the region is flat with mildly increasing dips at the bottom of the surveyed section (Lazaratos et al., 1992). The profile area is part of three 20-acre, five-spot patterns in a CO_2 pilot study.

A cylindrical piezoelectric bender was used as the source, with a linear upsweep from 250 to 2000 Hz. Well spacing is 184 ft (56 m). The receiver well in the crosswell profiling was an observation well drilled for the CO_2 study, and the receiver system was a nine-level array of hydrophones. The plane of the survey is almost perpendicular to the direction of natural fractures measured in a nearby well (Avasthi et al., 1991). The target of the experiment was a reservoir between 1850 and 1960 ft (564 and 597 m). Sources and receivers were centered around the reservoir, from 1650 to 2150 ft (503 to 655 m). (Reservoir depths are changed for purposes of presentation in this paper.) The vertical spacing between sources and receivers was 2.5 ft (0.8 m). The survey consists of nearly 36 000 traces (201 sources \times 178 receivers) sampled at 0.2 ms. More details about the data acquisition can be found in Harris et al. (1992).

Figure 9 shows a typical common-receiver gather. A clear P -wave direct arrival is visible for all vertical offsets. Direct

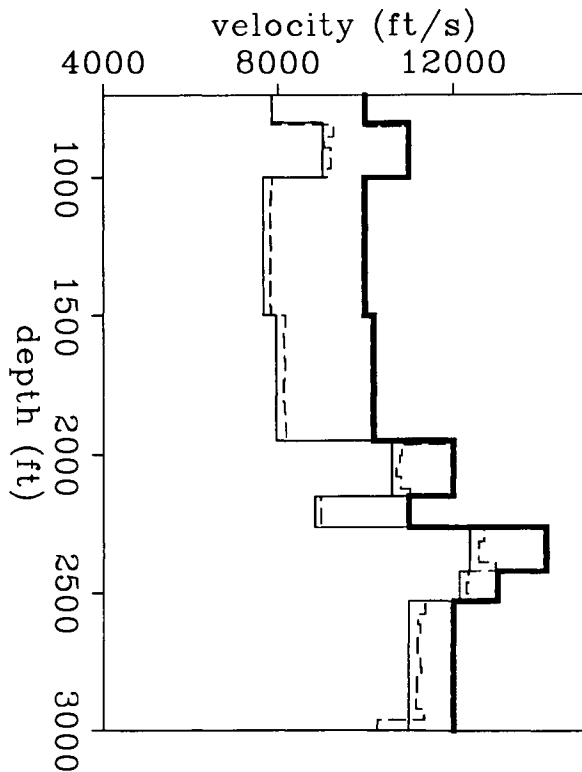


FIG. 4. P -wave elliptical velocities. Dashed lines: result of the inversion of P -wave traveltimes with a ray angle of less than 30°. Continuous lines: theoretical values. The curve with lower velocity corresponds to $V_{P,zNMO}$, and the one with higher velocity corresponds to $V_{P,x}$.

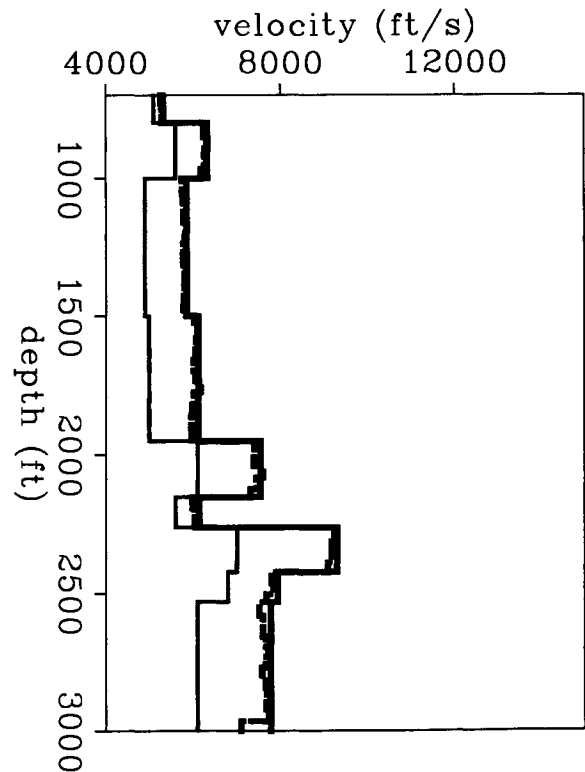


FIG. 5. SV -wave elliptical velocities. Dashed lines: result of the inversion of SV -wave traveltimes with a ray angle of less than 30°. Continuous lines: theoretical values. The curve with lower velocity corresponds to $V_{SV,x}$, and the one with higher velocity corresponds to $V_{SV,zNMO}$.

shear waves are not present at small vertical offsets but can be easily picked elsewhere, without having to do any special *P/S* separation. Van Schaack et al. (1992) show that the source can be modeled as a radial horizontal point source, which explains why no shear waves are clearly visible in the data for ray angles less than $\approx 28^\circ$ with respect to the horizontal, as Figure 9 shows. Data editing and geometry definition were performed before picking. The total number of traveltimes picked from the field data was 33 519 and 20 887 for *P*-waves and *S*-waves, respectively.

P-wave energy is converted to shear energy at the source well. If the source well is perfectly cylindrical and if the downhole source is positioned symmetrically within the source well, the polarization of the converted energy recorded at the receiver well is contained in the plane of the survey. Therefore, it is safe to assume that most of the recorded shear energy in this experiment corresponds to the *SV*-mode.

The *P*-wave traveltimes used for the inversion were from sources and receivers forming angles between 9 and 36° with the horizontal. Even though the corresponding range of ray angles may be slightly different depending on how strong the velocity contrasts are, we still expect most ray angles at all layers to fall within the range of validity of the elliptical approximation. By applying this constraint on the data aperture, the number of *P*-wave traveltimes was reduced to 12 258 from the original 33 519. For similar reasons, the

number of *S*-wave traveltimes was reduced to 2922, which corresponds to sources and receivers forming angles between 29 and 35° . The fact that only a small portion of the data set is used is a consequence of using an elliptical approximation as a basis to estimate the parameters that describe a more general TI medium.

The initial model for the tomographic inversion of *P*-wave traveltimes is homogeneous isotropic. The model is described by 200 horizontal layers of equal thickness and equal to the vertical spacing between sources and receivers (2.5 ft or 0.8 m). The total number of model parameters is 1000, and therefore, the problem is overdetermined. Figure 10 shows the elliptical velocities that result after inverting the data. $V_{P,zNMO}$ is larger than $V_{P,x}$ in some strata, which indicates that the anisotropy is not caused by fine, horizontal layering. The mean absolute value of the residuals for this model is 0.086 ms, less than half the sampling rate.

Figure 11 shows the elliptical velocities that result from the inversion of shear-wave traveltimes. The initial model in this case was also homogeneous isotropic and described by 200 layers of equal thickness. Seven layers were eliminated during the inversion procedure. $V_{SV,zNMO}$ is close to $V_{SV,xNMO}$, which means that the *P*-wave anisotropy at this site is close to elliptical. As Figures 10 and 11 show, the shear-wave anisotropy at this site is smaller than the compressional wave anisotropy. The mean absolute value of the residuals

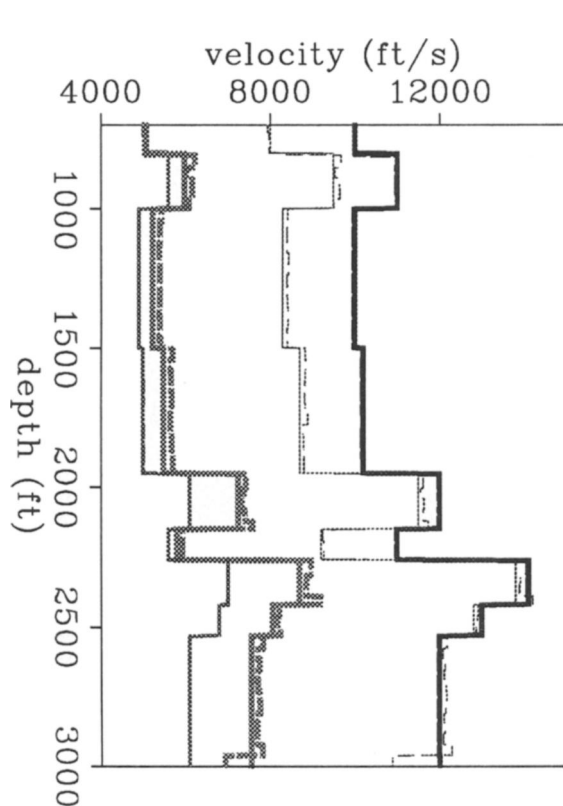


FIG. 6. Elastic constants that control *P*- and *SV*-wave propagation. Dashed lines: estimated. Continuous lines: given. From left to right the four pairs of curves represent V_{44} , V_{13} , V_{33} , and V_{11} , respectively.

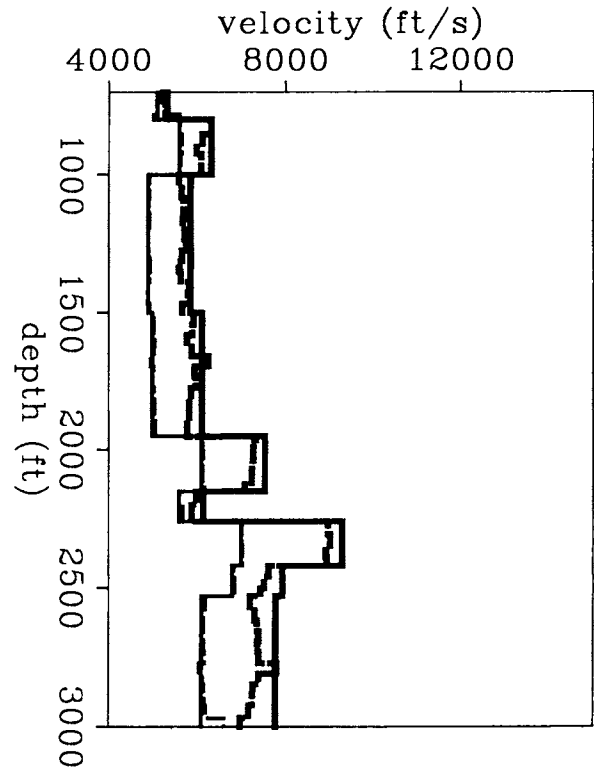


FIG. 7. *SV*-wave elliptical velocities. Dashed lines: result of the inversion of *SV*-wave traveltimes with ray angles between 28 and 36° . Continuous lines: theoretical *SV*-wave elliptical velocities. The curves with lower velocity correspond to $V_{SV,x}$ and the ones with higher velocity correspond to $V_{SV,zNMO}$.

computed for the model in Figure 11 is 0.240 ms, approximately equal to the sampling interval.

Finally, the elliptical velocities of Figures 10 and 11 are transformed into elastic constants at each depth. Figure 12 shows the result of the transformation. V_{11} and V_{33} (horizontal and vertical P -wave velocities, respectively) vary more rapidly than V_{44} (SV -wave velocity). V_{33} is almost the same as $V_{P,zNMO}$ because the shear-wave anisotropy is not significant as Figure 11 shows. The difference $V_{11} - V_{33}$ alternates between zero or negative in the interval between 1700 and 2100 ft (518 and 640 m). If we assume that the anisotropy is caused by fine layering, such changes in $V_{11} - V_{33}$ can be explained by a sequence of isotropic and anisotropic strata with horizontal axes of symmetry, probably caused by vertical fractures. The reservoir between 1850 and 1960 ft (564 and 597 m) corresponds to one stratum that is probably vertically fractured, which suggests that other intervals where $V_{11} < V_{33}$ may also correspond to vertically-fractured reservoir zones.

Figure 13 compares the horizontal and vertical velocities estimated from the crosswell measurements with the vertical shear and compressional velocities derived from the sonic log. Comparing shear-wave velocities yields the results expected for a TI medium: the vertical shear velocity from

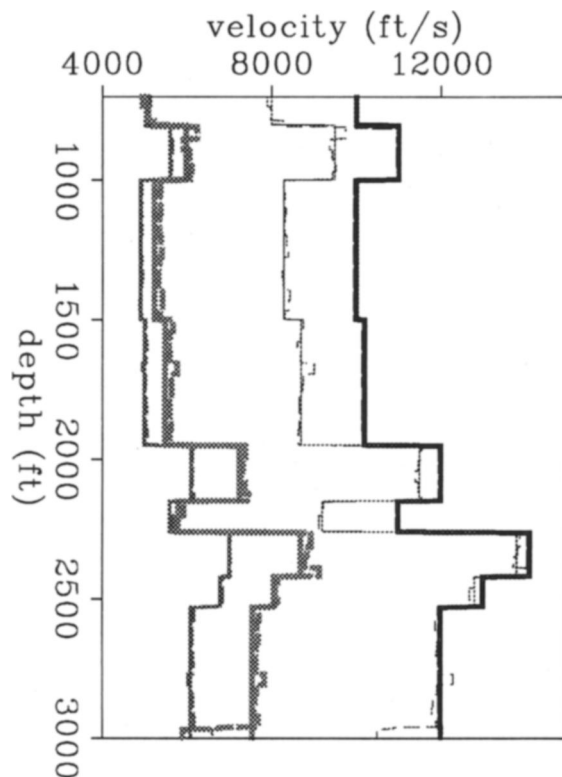


FIG. 8. Elastic constants that control P - and SV -wave propagation. Dashed lines: elastic constants estimated when the ray angles used in the tomographic inversion of SV -wave traveltimes are between 28 and 36°. The ray angles used to obtain the P -wave elliptical velocities are between 0 and 30° as in Figure 6. Continuous lines: original elastic constants. From left to right the four pairs of curves represent V_{44} , V_{13} , V_{33} , and V_{11} , respectively.

the sonic log is the same as the horizontal shear velocity derived from crosswell measurements. For the compressional velocities, however, the results are not as expected: the sonic log velocity is closer to the horizontal velocity than to the vertical velocity estimated from crosswell traveltimes. If we assume that the sizes of the heterogeneities in the interwell region and those close to the wells are the same, we expect the logs to yield equal or faster velocities than the crosswell measurements, even if the medium is isotropic. The reason for this difference is that the waves generated by sonic tools travel faster because they contain higher frequencies. Our results show exactly the opposite in the zones that are probably vertically fractured.

We have three hypotheses to explain these differences. The first one, and also the simplest, assumes that the sonic logs were recorded before the reservoir was stimulated by hydraulic fracturing. If this is the case, which we could not confirm, the hydraulic fractures could have produced an increase in the vertical P -wave velocity (derived from crosswell measurements) which was not recorded by the log. The second hypothesis assumes that fluids used when drilling can

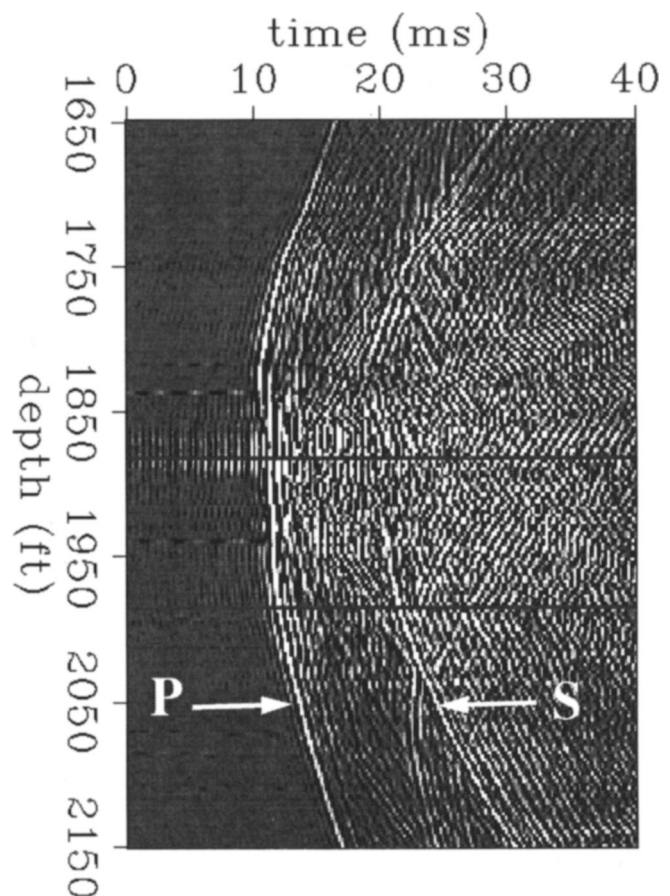


FIG. 9. Common-receiver gather recorded at 1880 ft (573 m). The source depth interval is 2.5 ft (0.8 m). The well-to-well separation is 184 ft (56 m). First arriving compressional (P) and shear (S) waves are clearly visible at most vertical offsets. Other wave modes are also visible. The target of the experiment was a reservoir between 1850 and 1960 ft (564 and 597 m).

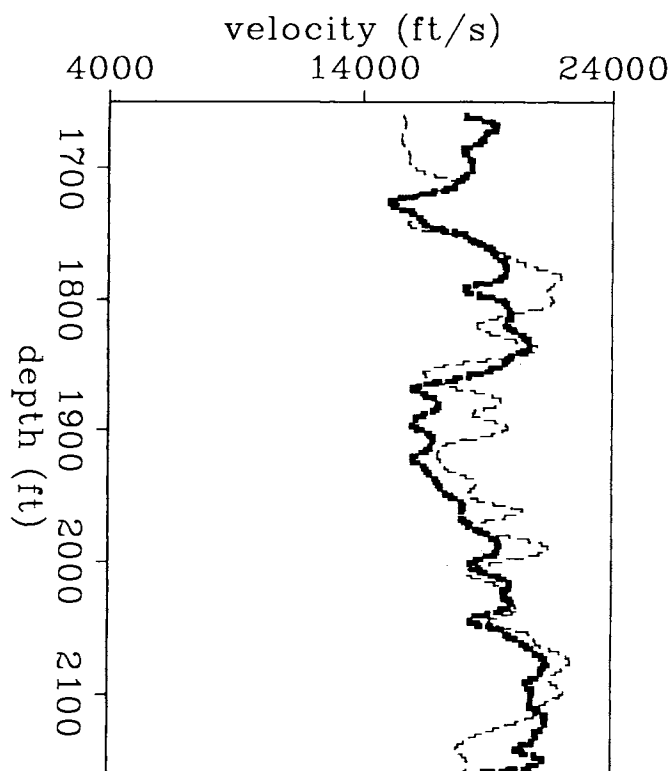


FIG. 10. P -wave elliptical velocities estimated from field data. Thick line: $V_{P,x}$. Thin line: $V_{P,zNMO}$. The model is described by 200 horizontal layers.

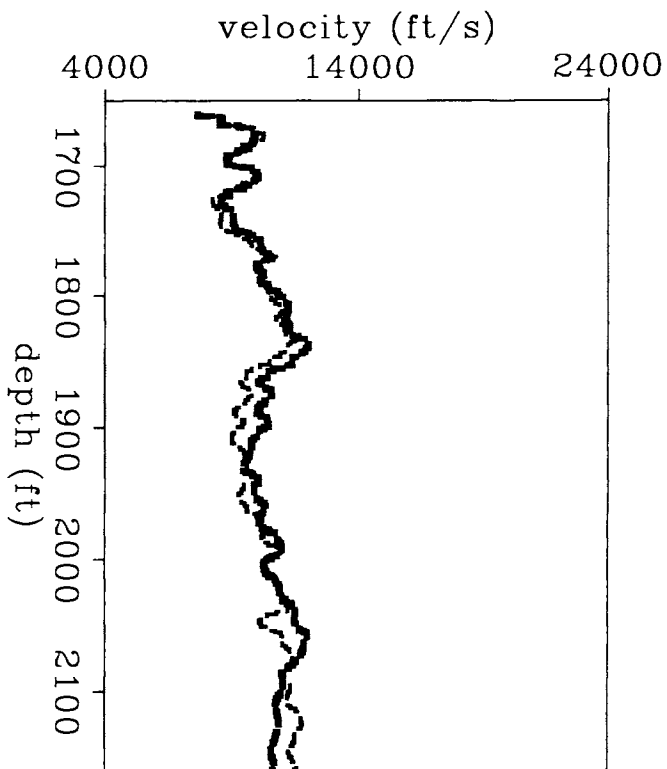


FIG. 11. S -wave elliptical velocities estimated from field data. Thick line: $V_{SV,zNMO}$. Thin line: $V_{SV,x}$. The model is described by 193 horizontal layers.

penetrate the reservoir zones (probably vertically fractured) causing a decrease in the compressional velocities of waves that travel close to the well without affecting either the velocities of waves that travel far from the well or the shear velocities. The third hypothesis acknowledges that the velocity model might be inadequate because it does not account for lateral velocity variations. Strong, lateral heterogeneities in the vertical component of the velocity may cause the type of behavior observed in the results because the model does not account for those variations. This possibility, however, is less likely because reflection images of the site show fairly laterally homogeneous layers (Lazaratos et al., 1992).

Having out-of-plane shear arrivals would help to confirm the hypothesis of vertical fractures by allowing us to look at the shear-wave splitting in the near horizontal direction.

CONCLUSIONS

The procedures used to estimate elastic constants in heterogeneous TI media is a generalization of the technique presented in Michelena (1994) for estimating elastic constants in homogeneous TI media. For homogeneous media, traveltimes from different wave types are fitted with elliptically anisotropic models. The elliptical velocities that result are then transformed into elastic constants. For heterogeneous media, the elliptical fit is performed by using aniso-

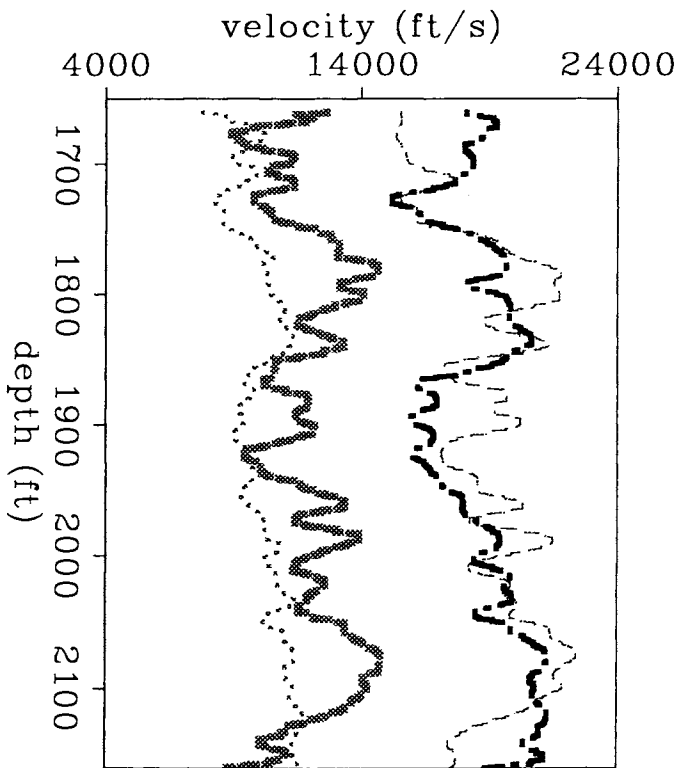


FIG. 12. Elastic constants at the McElroy site (in units of velocity) estimated from the elliptical velocities of Figures 10 and 11, assuming a TI medium. Dotted line: V_{44} . Thick-dashed line: V_{13} . Dotted-dashed line: V_{11} . Thin-dashed line: V_{33} .

tropic traveltimes tomography, and the transformation to elastic constants is performed locally at each point in space.

The examples presented in this paper show that the procedure is accurate as long as the maximum aperture satisfies the following constraints: the aperture must not be too small because that would impede the estimation of the NMO velocities, and it must not be too large because the elliptical approximation might not be adequate. These two constraints are analogous to the constraints on the offsets in surface geometries when estimating rms velocities from stacking velocities.

The consequences of the constraints on the data are twofold. First, part of the data may not be used if they do not have the required aperture and, unfortunately, these data that are not used do not necessarily contain redundant information. Second, the range of dips and inclinations of the axes of symmetry of the medium that can be accurately estimated is reduced if the data cannot be explained by elliptical models. This means that when the apertures are constrained by assuming that the inclination of the axes of symmetry of the medium are close to vertical or close to horizontal, only small dips can be well estimated and, consequently, the structures are assumed to be nearly layered. Although these assumptions seem too restrictive, we should remember that the assumption of layered structures

with vertical axes of symmetry has been a common one for years in problems of velocity estimation. Moreover, when the medium is anisotropic, the assumption of isotropy and arbitrary 2-D variations may be worse than the assumption of anisotropic layered models (Michelena et al., 1993).

In this paper, we tested the algorithm with simple layered models. The estimation of elastic constants in media with more complex heterogeneities may require traveltimes from wider apertures, which could yield less accurate results. This problem can be solved by using traveltimes from all wave types from different recording geometries.

The constraints on the aperture may be softened by using approximations more general than elliptical. Dellinger et al. (1993) propose a three-parameter anelliptic approximation that might be used for this purpose. However, more research needs to be done to determine how to transform these three parameters into the elastic constants of the medium.

ACKNOWLEDGMENTS

The field data, picked and edited by Mark Van Schaack, was recorded by the Seismic Tomography Project. Thanks to Chevron Petroleum Technology that made their field site available to Stanford. We thank David Lumley and Richard Nolen-Hoeksema for their useful comments. Intevp, S.A. provided financial support to the first author while attending Stanford University.

REFERENCES

- Al-Chalabi, M., 1973, Series approximation in velocity and travel-time computations: *Geophys. Prosp.*, **21**, 783-795.
- Auld, B. A., 1990, *Acoustic fields and waves in solids*, Vol. 1: Robert E. Krieger Publishing Co.
- Avasthi, J. M., Nolen-Hoeksema, R. J., and El Rabaa, A. W. M., 1991, In-situ stress evaluation of the McElroy Field, west Texas: *SPE Formation Eval.*, September issue, 301-309.
- Carrion, P., Costa, J., Ferrer Pinheiro, J. E., and Schoenberg, M., 1992, Cross-borehole tomography in anisotropic media: *Geophysics*, **57**, 1194-1198.
- Chapman, C. H., and Pratt, R. G., 1992, Traveltime tomography in anisotropic media-I. Theory: *Geophys. J. Intl.*, **109**, 1-19.
- Dellinger, J., Muir, F., and Karrenbach, M., 1993, Anelliptic approximations for TI media: *J. Seismic Expl.*, **2**, 23-40.
- Harris, J. M., Nolen-Hoeksema, R., Rector, J. W., Van Schaack, M., and Lazaratos, S. K., 1992, High-resolution, cross-well imaging of a west Texas carbonate reservoir: Part 1. Data acquisition and project overview: 62nd Ann. Internat. Mtg., Soc. Expl. Geophys., Expanded Abstracts, 35-39.
- Lazaratos, S. K., Harris, J. M., Rector, J. W., and Van Schaack, M., 1992, High-resolution, cross-well imaging of a west Texas carbonate reservoir, Part 4: Reflection imaging: 62nd Ann. Internat. Mtg., Soc. Expl. Geophys., Expanded Abstracts, 49-53.
- Lines, L., 1992, Poor's man anisotropic traveltime tomography: 62nd Ann. Internat. Mtg., Soc. Expl. Geophys., Expanded Abstracts, 83-86.
- McCann, C., Assefa, S., Sothcott, J., McCann, D. M., and Jackson, P. D., 1989, In-situ borehole measurements of compressional- and shear-wave attenuation in Oxford clay: *Sci. Drilling*, **1**, 11-20.
- Michelena, R. J., 1993, Anisotropic traveltime tomography: Ph.D thesis, Stanford University.
- Michelena, R. J., Muir, F., and Harris, J. M., 1993, Anisotropic traveltime tomography: *Geophys. Prosp.*, **41**, 381-412.
- Michelena, R. J., 1994, Elastic constants of transversely isotropic media from constrained aperture traveltimes: *Geophysics*, **59**, 658-667.
- Pratt, R. G., and Chapman, C. H., 1992, Traveltime tomography in anisotropic media-II. Application: *Geophys. J. Intl.*, **109**, 20-37.
- Qin, F., Luo, Y., and Cai, W., 1992, Traveltime inversion for anisotropic seismic data: 62nd Ann. Internat. Mtg., Soc. Expl. Geophys., Expanded Abstracts, 762-765.

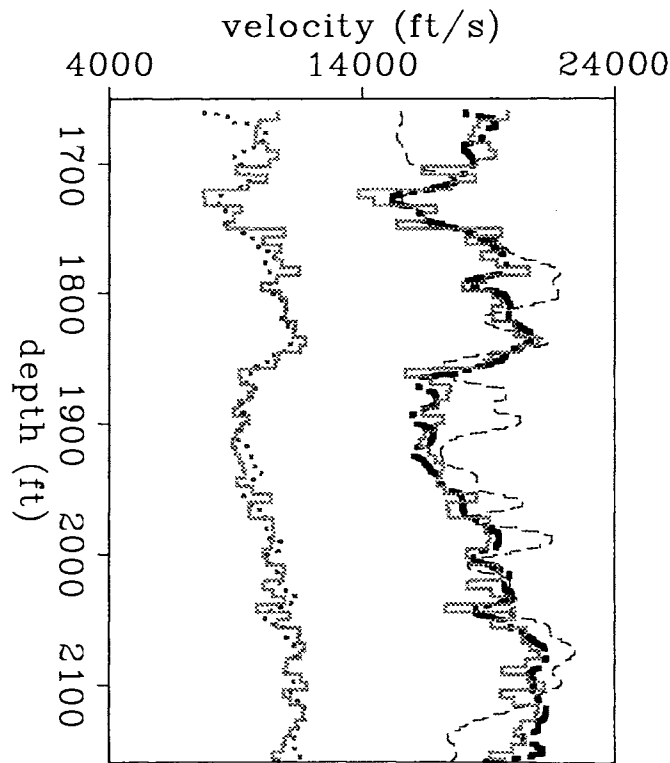


FIG. 13. Elastic constants (in units of velocity) estimated from crosswell traveltimes compared with sonic logs blocked every 6 ft (1.8 m). Continuous line at the left: shear sonic velocity. Continuous line at the right: compressional sonic velocity. Dotted line: V_{44} . Dotted-dashed line: V_{11} . Thin-dashed line: V_{33} .

- Saito, H., 1991, Anisotropic travelttime tomography at the Buckhorn test facility in Illinois: 62nd Ann. Internat. Mtg., Soc. Expl. Geophys., Expanded Abstracts, 123–126.
- Stewart, R. R., 1988, An algebraic reconstruction technique for weakly anisotropic velocity: *Geophysics*, **53**, 1613–1615.
- Thomsen, L., 1986, Weak elastic anisotropy: *Geophysics*, **51**, 1954–1966.
- Van Schaack, M., Harris, J. M., Rector, J. W., and Lazaratos, S. K., 1992, High-resolution, cross-well imaging of a west Texas carbonate reservoir, Part 2: Wave-field analysis and tomography: 62nd Ann. Internat. Mtg., Soc. Expl. Geophys., Expanded Abstracts, 40–44.
- Williamson, P. R., Sams, M. S., and Worthington, M. H., 1993, Crosshole imaging in anisotropic media: *The Leading Edge*, **12**, 19–23.
- Yilmaz, O., 1987, Seismic data processing, Soc. Expl. Geophys.